RSC Advances

PAPER

View Article Online
View Journal | View Issue

Cite this: *RSC Adv.*, 2020, **10**, 9902

ALD Al_2O_3 gate dielectric on the reduction of interface trap density and the enhanced photoelectric performance of IGO TFT

Kuan-Yu Chen,[ab] Chih-Chiang Yang,*[b] Chun-Yuan Huang*[c] and Yan-Kuin Su[ab]

Received 6th January 2020
Accepted 21st February 2020

DOI: 10.1039/d0ra00123f

rsc.li/rsc-advances

The amorphous indium gallium oxide thin film transistor was fabricated using a cosputtering method. Two samples with different gate dielectric layers were used as follows: sample A with a SiO_2 dielectric layer; and sample B with an Al_2O_3 dielectric layer. The influence of the gate dielectrics on the electric and photo performance has been investigated. Atomic layer deposition deposited the dense film with low interface trapping density and effectively increased drain current. Therefore, sample B exhibited optimal parameters, with an I_{on}/I_{off} ratio of 7.39×10^7, the subthreshold swing of 0.096 V dec^{-1}, and μ_{FE} of 5.36 cm^2 V^{-1} s^{-1}. For ultraviolet (UV) detection, the UV-to-visible rejection ratio of the device was 3×10^5, and the photoresponsivity was 0.38 A W^{-1} at the V_{GS} of −5 V.

Introduction

Amorphous oxide semiconductors on the basis of thin film transistors have been widely developed in active matrix liquid crystal displays, optoelectronic, and organic light-emitting-diode displays.[1–3] Among these amorphous oxide semiconductors, In_2O_3-based TFTs have attracted considerable attention and were investigated due to their high electron mobility and transparency.[4–7] Nevertheless, the In concentration in the active channel layer is relatively high, thereby impeding device performance. Excess In_2O_3 content produces excess oxygen vacancies in the channel layer. Parthiban *et al.*[8] reported metal cations as carrier suppressors and strong bonders; they control the oxygen defect concentration, according to the bond strength of metal oxide, which can improve and enhance the performance of the device. Hsu *et al.*[9] reported fabrication of an indium titanium zinc oxide TFT and manipulated the O flow ratio during sputtering, which suppresses the excess oxygen vacancies in the active layer. With the increase in O flow ratio, the device performance is improved. Our group previously reported the cosputtering of the indium gallium oxide (IGO) thin film with different deposition powers of the In_2O_3 target, and the photo and electric properties showed that oxygen vacancies are strongly dependent on the In content.[10] According to the relevant study results, the In_2O_3-based TFTs improved the device performance by different methods. However, these methods degrade the mobility and I_{on}/I_{off} ratio. Hence, we prepared Al_2O_3 as the gate dielectric to optimize the photo and electric properties. Given the advantages of atomic layer deposition (ALD), such as uniformity and control of deposition, the thin film that is generally used for high k materials or passivation layer for TFTs has low leakage current and interface state densities.[11,12] High-k materials, such as Si_3N_4 (∼7), Al_2O_3 (∼9), MgO (∼9.8), La_2O_3 (∼14), and ZrO_x (∼15), which increase the drain current due to their high dielectric constant values, improve the transistor device characteristics.[13–19] In the present study, the IGO thin film transistor was investigated with different dielectrics. Sample A used SiO_2 as a dielectric by wet oxidation. Sample B used Al_2O_3 as a dielectric prepared by ALD. The IGO thin films with large energy band gap were prepared by radio frequency magnetron sputtering system and can be used for ultraviolet (UV) sensing. The detailed photo and electric performances of the devices are discussed in the following sections.

Device fabrication and characterization

The fabricated samples comprised a Si substrate, a dielectric layer, IGO thin films, and source/drain Al electrodes. Two samples with different dielectric layers were used, as follows: sample A with SiO_2 as dielectric layer; and sample B with Al_2O_3 as dielectric layer. First, the heavily doped p-type Si substrate was ultrasonically cleaned with acetone, methanol, and water for 10 min. Afterward, sample A was grown on a 300 nm SiO_2 layer by a wet-oxide tube. Meanwhile, sample B was fabricated on a 70 nm Al_2O_3 dielectric layer by ALD deposition with precursor trimethylaluminum (TMA) and H_2O. The duration times of precursor A (TMA), purge, precursor B (H_2O), and purge

[a]*Department of Electrical Engineering, Institute of Microelectronics, National Cheng Kung University, Tainan 701, Taiwan*
[b]*Green Energy Technology Research Center, Department of Electrical Engineering, Kun Shan University, Yongkang 710, Taiwan. E-mail: 298r.yang@gmail.com*
[c]*Department of Applied Science, National Taitung University, Taitung 950, Taiwan. E-mail: laputa@nttu.edu.tw*

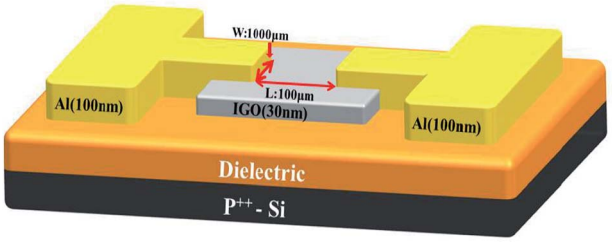

Fig. 1 Scheme of IGO TFTs.

were 0.1, 4.0, 0.1, and 6.0 s, respectively. The growth rate was 0.094 nm per cycle at 250 °C deposition temperatures.

The IGO channel layer was deposited by cosputtering using Ga_2O_3 and In_2O_3 targets with 100 W Ga_2O_3 power and 60 W In_2O_3 power, respectively. The growth pressure was fixed on 6 mTorr, with an Ar flow ratio of 3 sccm. The thickness of the channel layer was 30 nm. Afterward, the thin film that was annealed in Ar flow for 60 min at 300 °C. Finally, the Al electrodes were grown at 100 nm using a shadow mask by thermal evaporation. The channel length and width were 100 and 1000 μm, respectively. The electric properties were measured by Agilent B1500 under dark conditions. A 150 W Xe lamp was used to measure the photo properties. The scheme of the IGO TFTs is shown in Fig. 1.

Results and discussion

Fig. 2 reveals the optical band gap energy of the IGO active layer as calculated by the Tauc plot, which can be extracted by the following equation:

$$(\alpha h\nu)^2 = C(h\nu - E_g) \quad (1)$$

where α is the absorbance, E_g is the band gap, and C is the constant. The energy band gap of the IGO thin film is approximately at 4 eV, and the corresponding cut-off wavelength was ~310 nm. The inset figure shows the transmittance spectra. The films were highly transparent, with over 80% visible region.

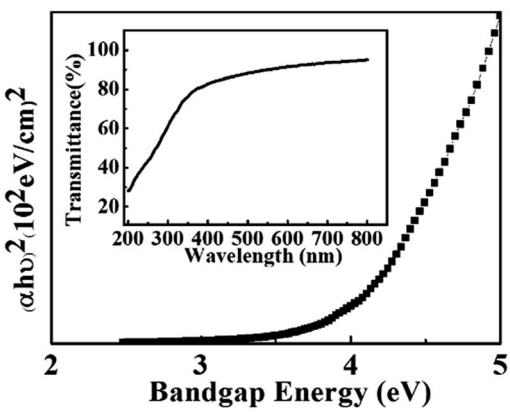

Fig. 2 Tauc plot of IGO thin film deposited at 300 °C on quartz glass. The inset figure shows the optical transmittance spectra of the IGO thin films.

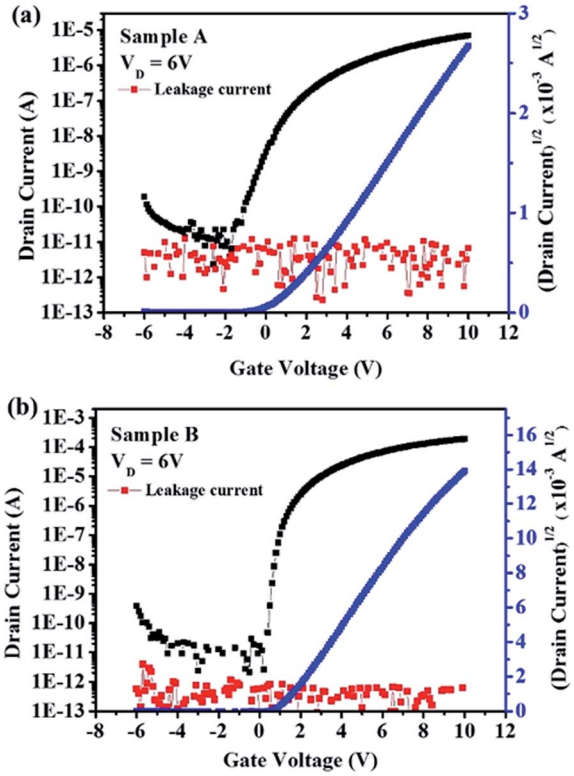

Fig. 3 Measured transfer characteristics and measured leakage current of (a) sample A and (b) sample B, with different dielectric layer.

Fig. 3(a) and (b) show the transfer curves and leakage current of samples A and B, respectively, and the extraction averaged value of the two device parameters are listed in Table 1. Two devices were operated in n-type enhancement mode. The threshold voltage was extrapolated from the linear $(I_{DS})^{1/2}$–V_{GS} curve. The two devices have very low leakage current value approximately at 10^{-12} Å which value was negligible. The threshold voltages of sample A and B were 0.8 and 1.3 V, respectively.

The field effect mobility (μ_{EF}) and subthreshold swing (SS) can be obtained by the following equations:[20]

$$I_D = \frac{W}{2L} C\mu_{EF}(V_G - V_T)^2 \quad (2)$$

$$SS = \frac{\partial V_{GS}}{\partial \log(I_{DS})} \quad (3)$$

where C is the capacitance of the dielectric layer, W/L is the channel width and length, V_T is the threshold voltage, and μ is the saturation mobility. SS is defined as the change in the gate voltage required to increase the drain current by one decade (from 10^{-10} Å to 10^{-9} Å). The μ_{EF} values of samples A and B were 1.83 and 5.36 $cm^2\ V^{-1}\ s^{-1}$, and their SS values were 1.2 and 0.096 V dec^{-1}, respectively. The I_{on}/I_{off} ratio that increased by two orders of magnitude were substituted with an Al_2O_3 dielectric layer. The output characteristics of the two samples with different dielectric layers as a function of the gate overdrive voltage are shown in Fig. 4. Under the same gate bias, sample B

Table 1 An extraction averaged value of the IGO TFTs with variable dielectric layer

	I_{on}/I_{off} ratio ($\times 10^5$)	SS (V dec^{-1})	μ_{FE}(cm^2 V^{-1} s^{-1})	V_{TH} (V)	N_t (cm^{-2} eV^{-1}) ($\times 10^{11}$)
Sample A	5.58 ± 2	1 ± 0.25	1.71 ± 0.34	0.6 ± 0.18	12.4 ± 1.7
Sample B	460 ± 260	0.1 ± 0.04	5.11 ± 0.35	1.4 ± 0.25	5.89 ± 3.2

had a higher saturation current compared with sample A, which can attribute the higher dielectric constant. The saturation current of sample A and sample B were 6.25 μA and, 101 μA, respectively. To characterize the interface state density at the channel/dielectric layer, the interface-state trap density (N_{ss}) can be obtained through the following equation:[21]

$$N_{ss} = \left[\frac{SS \log_{(e)}}{(kT/q)} - 1\right] \frac{C_i}{q} \quad (4)$$

where k is the Boltzmann constant, q is the electron charge, T is the temperature, and is the insulator capacitance per unit area. The interface-state trap densities of samples A and B were 1.37 $\times$ 10^{12} and 7.50 $\times$ 10^{11} cm^{-2} eV^{-1}, respectively. The interface trapping density was effectively reduced by the Al_2O_3 layer. The less interface-state trap in sample B could be credited for the dense and uniformity of Al_2O_3 dielectric layer obtained through the ALD deposition process. Moreover, compared with the wet-oxide tube-grown SiO_2 dielectric layer, the Al_2O_3 dielectric layer showed comparative uniformity.

Hence, the hysteresis properties should be improved due to the quality of the dielectric, thereby reducing the N_{ss}. Hysteresis loop measured by sweeping the gate voltage from −6 V to 10 V back and forth. The ΔV_T values of samples A and B were 1.4 and 0.3 V, respectively. The large hysteresis of sample A indicated the presence of interface states in the SiO_2 layer and that the hysteresis was suppressed in sample B (Fig. 5).

As discussed above, the optical energy bandgap of the IGO active layer was approximately at 4 eV, with a corresponding cut-

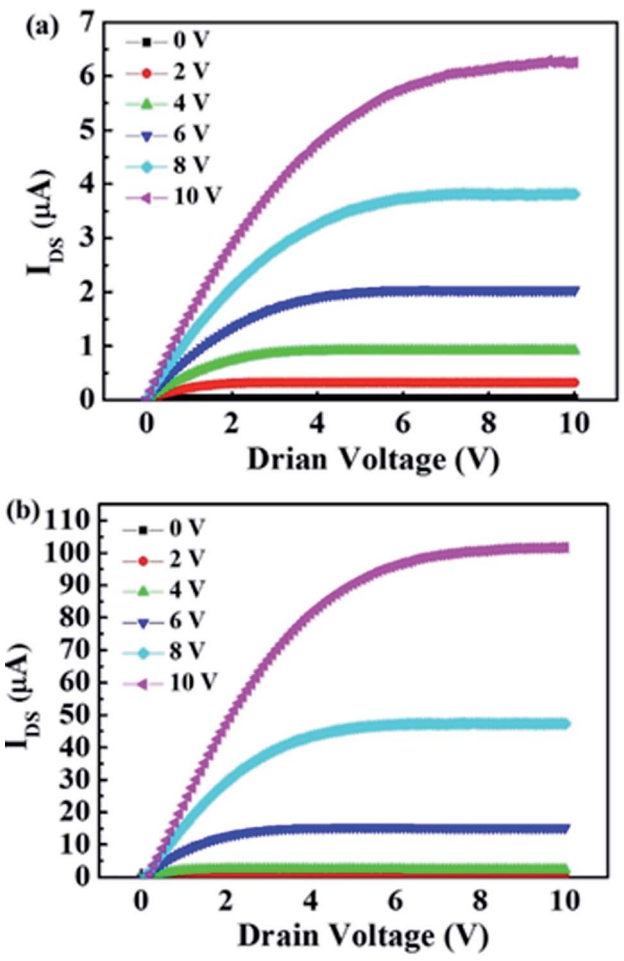

Fig. 4 Measured output characteristics of (a) sample A and (b) sample B, with different dielectric layer.

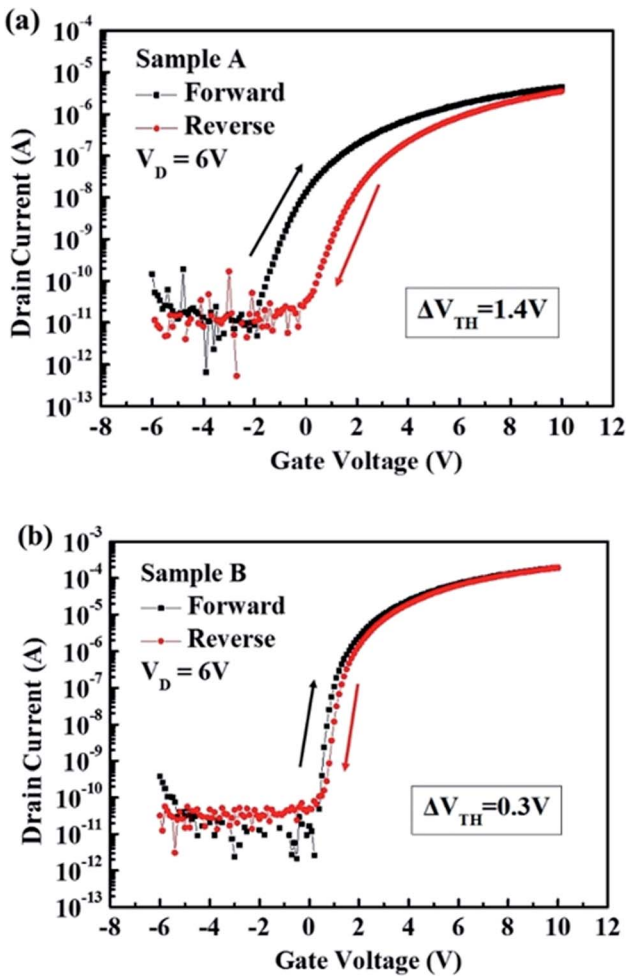

Fig. 5 Hysteresis of transfer characteristics of (a) samples A and (b) B, in which sweep range of gate voltage was −6 V from 10 V.

off wavelength of 300 nm. Hence, the IGO active layer has considerable potential as a candidate for UV detection application. Fig. 6 depicts the transfer characteristics of samples A and B, which were measured using a Xe lamp at the wavelength ranging from 480 nm to 250 nm under illumination. The transfer curve from a negative direction moved when the illumination head for short wavelength due to the induced photogenerated carrier, and the light and dark currents increased. The I_{DS} increased possibly due to the following reasons; the photogenerated carrier in the IGO thin film caused by optical absorption; and the fact that ionized V_o can act as a shallow donor state, thereby leading band-to-band excitation under visible illumination, as generally indicated for amorphous oxides.[22,23] Consequently, the drain current increased, and the V_{TH} shifted in the negative direction, which can be attributed to carrier generation due to optical absorption and also due to the fact that high dielectric constant can increase the drain current.

The photoresponsivity of the two samples are shown in Fig. 7. The responsivity can be calculated by the following equation:

$$R = \frac{I_{photo} - I_{dark}}{P_{opt}} \quad (5)$$

where I_{photo} is the photocurrent, I_{dark} is the dark current, and P_{opt} indicates the light power. The corresponding responsivities

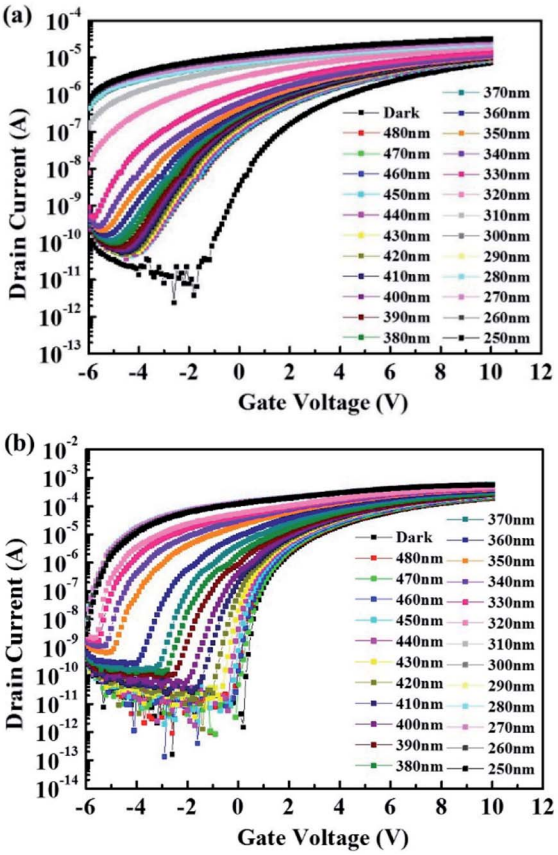

Fig. 6 Transfer characteristics of (a) sample A and (b) sample B measure in the dark condition and under illumination with various light wavelength (480 nm to 250 nm).

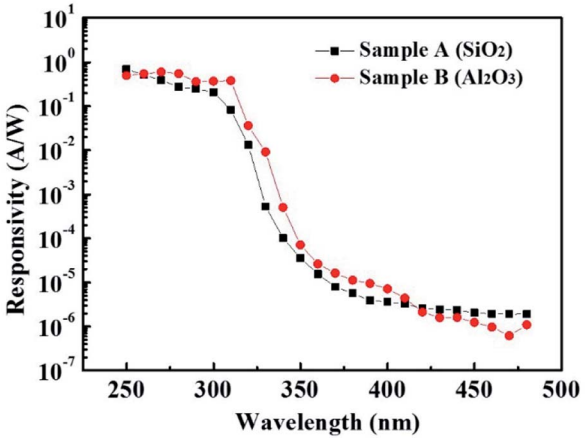

Fig. 7 The responsivity of sample A and sample B were measured at various wavelength and VGS of −5 V.

Table 2 Photo responsivity and UV-vis of two samples with different dielectric layer

	Responsivity (A W^{-1}) @ 310 nm	UV-vis
Sample A	0.08	4×10^4
Sample B	0.38	3×10^5

(310 nm) of samples A and B were 0.08 and 0.38 A W^{-1}, respectively. Sample B exhibited improved response under UV illumination. This result can be attributed to the fact that Al_2O_3 dielectric layer had less trap states and increased gate dielectric constant. UV-to-visible rejection ratio (UV-vis) is the responsivity measured at the peak wavelength of 310 nm divided by the responsivity measured at 450 nm. The UV-vis values of samples A and B were 4×10^4 and 3×10^5, respectively. Although sample B exhibited good rejection ratio, sample A had excellent rejection ratio, and the two samples were effectively identified through UV radiation. To prepare the IGO thin film transistor with different dielectric layers, we improved the photo and electric performances by replacing the Al_2O_3 dielectric layer. The IGO TFTs can act as a UV phototransistor (Table 2).

Conclusions

The IGO thin film transistors were investigated with different dielectric layers using SiO_2 and Al_2O_3 (samples A and B, respectively). The influence of the dielectric layer on electrical and photo characteristics has been investigated. The output characteristics shows that a higher dielectric constant can increase the drain current. The N_{ss} was suppressed, which also improved the hysteresis loop, indicated that the interface trapping density effectively reduced *via* atomic layer deposition. In addition, the device had a UV-vis of 3×10^5, a photoresponsivity of 0.38 A W^{-1} under a V_{GS} value of −5 V in the 310 nm wavelength region, which is suitable for UV sensing application.

Conflicts of interest

There are no conflicts to declare.

Acknowledgements

This work was supported in part by the Ministry of Science and Technology of Taiwan, ROC, under Grant MOST 107-2221-E-006-185-MY3 and Grant 108-2221-E-006-201-MY3, and in part by the Green Energy Technology Research Center, Department of Electrical Engineering, Kun Shan University, Tainan, Taiwan through The Featured Areas Research Center Program within the framework of the Higher Education Sprout Project by the Ministry of Education (MOE) in Taiwan.

References

1 L. Zhang, W. Xiao, W. Wu and B. Liu, *Appl. Sci.*, 2019, **9**, 773.
2 X. Yu, T. J. Marks and A. Facchetti, *Nat. Mater.*, 2016, **15**, 383–396.
3 H. Hosono, J. Kim, Y. Toda, T. Kamiya and S. Watanabe, *Proc. Natl. Acad. Sci. U. S. A.*, 2017, **114**, 233–238.
4 J. Smith, L. Zeng, R. Khanal, K. Stallings, A. Facchetti, J. E. Medvedeva, M. J. Bedzyk and T. J. Marks, *Adv. Electron. Mater.*, 2015, **1**, 1500146.
5 N. Mitoma, S. Aikawa, X. Gao, T. Kizu, M. Shimizu, M.-F. Lin, T. Nabatame and K. Tsukagoshi, *Appl. Phys. Lett.*, 2014, **104**, 102103.
6 H. Zhang, Y. Meng, L. Song, L. Luo, Y. Qin, N. Han, Z. Yang, L. Liu, J. C. Ho and F. Wang, *Nano Res.*, 2018, **11**, 1227–1237.
7 Q. Ma, H. M. Zheng, Y. Shao, B. Zhu, W. J. Liu, S. J. Ding and D. W. Zhang, *Nanoscale Res. Lett.*, 2018, **13**, 4.
8 S. Parthiban and J.-Y. Kwon, *J. Mater. Res.*, 2014, **29**, 1585–1596.
9 M. H. Hsu, S. P. Chang, S. J. Chang, W. T. Wu and J. Y. Li, *Nanomaterials*, 2017, **7**, 156.
10 K. Y. Chen, C. C. Yang, Y. K. Su, Z. H. Wang and H. C. Yu, *Materials*, 2019, **12**, 737.
11 P. O. Oviroh, R. Akbarzadeh, D. Pan, R. A. M. Coetzee and T. C. Jen, *Sci. Technol. Adv. Mater.*, 2019, **20**, 465–496.
12 B. Wang, W. Huang, L. Chi, M. Al-Hashimi, T. J. Marks and A. Facchetti, *Chem. Rev.*, 2018, **118**, 5690–5754.
13 W. J. Scheideler, M. W. McPhail, R. Kumar, J. Smith and V. Subramanian, *ACS Appl. Mater. Interfaces*, 2018, **10**, 37277–37286.
14 C.-H. Lee, N. Vardy and W. Wong, *IEEE Electron Device Lett.*, 2016, 1, DOI: 10.1109/led.2016.2557231.
15 P. Gogoi, R. Saikia, D. Saikia, R. P. Dutta and S. Changmai, *Phys. Status Solidi*, 2015, **212**, 826–830.
16 G. Jiang, A. Liu, G. Liu, C. Zhu, Y. Meng, B. Shin, E. Fortunato, R. Martins and F. Shan, *Appl. Phys. Lett.*, 2016, **109**, 183508.
17 L. Zhu, G. He, J. Lv, E. Fortunato and R. Martins, *RSC Adv.*, 2018, **8**, 16788–16799.
18 W. He, W. Xu, Q. Peng, C. Liu, G. Zhou, S. Wu, M. Zeng, Z. Zhang, J. Gao, X. Gao, X. Lu and J. M. Liu, *J. Phys. Chem. C*, 2016, **120**, 9949–9957.
19 N. E. I. Boukortt, B. Hadri and S. Patanè, *Int. J. Comput. Sci. Appl.*, 2016, 139.
20 T. C. Fung, C. S. Chuang, K. Nomura, H. P. D. Shieh, H. Hosono and J. Kanicki, *J. Inf. Disp.*, 2008, **9**, 21–29.
21 W. Shi, Y. Zheng, J. Yu, A. D. Taylor and H. E. Katz, *Appl. Phys. Lett.*, 2016, **109**, 143301.
22 S. Jeon, I. Song, S. Lee, B. Ryu, S. E. Ahn, E. Lee, Y. Kim, A. Nathan, J. Robertson and U. I. Chung, *Adv. Mater.*, 2014, **26**, 7102–7109.
23 L. S. Feng, G. Y. Yu, X. F. Li, J. H. Zhang, Z. Z. Ye and J. G. Lu, *IEEE Trans. Electron Devices*, 2017, **64**, 206–210.

